Showcasing research from Professor Fayan Zhu's laboratory, Key Laboratory of Green and High-end Utilization of Salt Lake Resources, Qinghai Institute of Salt Lakes, Chinese Academy of Sciences, Xining 810008, China.

Deciphering the structure and potassium-ion transport mechanism of potassium borate glass

The ion transport rate is closely related to the microstructure of the glass. By comparing the structure and properties of potassium borate glass and the crystals of similar components, the bond lengths of ^{3}B–BO (BO, bridging oxygen), ^{4}B–BO and ^{3}B–NBO (NBO, non-bridging oxygen) are longer than those of corresponding crystals, which leads to the structure of the boron–oxygen network being looser and the density is smaller than that of similar crystals. The key structures affecting the transport rate of K^{+} were NBO, chain structure units and cavities.

As featured in:

See Wu Li, Fayan Zhu *et al.*, *Dalton Trans.*, 2024, **53**, 10434.

ROYAL SOCIETY OF CHEMISTRY

rsc.li/dalton

Registered charity number: 207890

Dalton Transactions

ROYAL SOCIETY OF CHEMISTRY

PAPER

View Article Online
View Journal | View Issue

Cite this: *Dalton Trans.*, 2024, **53**, 10434

Deciphering the structure and potassium-ion transport mechanism of potassium borate glass†

Lulu Song,[a,b] Alex C. Hannon,[c] Steve Feller,[d] Ruirui Liu,[a] Peyton McGuire,[d] Bo Zhang,[a] Yongquan Zhou,[a] Wu Li *[a] and Fayan Zhu *[a]

Potassium borate glass has great potential as an ion transport material. The ion transport rate is closely related to the microstructure of the glass. However, the disorder and variations in boron and oxygen atom types in the glass structure pose challenges in the analysis of this complex glass structure. In this work, the structure of potassium borate glass was unveiled through the neutron diffraction method and *ab initio* molecular dynamics (AIMD) simulations. The B–O, K–O, and O–O atomic interactions, bond lengths, coordination numbers, cavity distribution, ring structure distributions and other detailed information in the microstructure of potassium borate glass were obtained. By comparing the structure and properties of potassium borate glass with those of crystals of similar components, it is found that the bond lengths of ^{3}B–BO (BO, bridging oxygen), ^{4}B–BO and ^{3}B–NBO (NBO, non-bridging oxygen) are longer than those of corresponding crystals, so the structure of the boron–oxygen network is looser and the density is smaller than that of similar crystals. Moreover, we found a rule that in both borate glass and crystal, the increase of NBO shortened the length of the B–O bond, and the increase of ^{4}B increased the length of the B–O bond. The key structures affecting the transport rate of K^{+} were NBO, chain structure units and cavities. This work will provide reference data for designing and developing electrically conductive amorphous materials with faster potassium-ion transport rates.

Received 18th March 2024,
Accepted 25th April 2024

DOI: 10.1039/d4dt00804a

rsc.li/dalton

1. Introduction

Potassium borate glass is widely used as a glass-forming agent,[1–5] which can be utilized to design and prepare new materials with potential applications in optics, electrochemistry, radiation shielding, *etc*. Alkali metal borate glass exhibits excellent nonlinear optical properties,[6] and the borate groups composed of B–O–B bonds contribute to enhancing the optical characteristics of glasses.[7] Currently, radiation shielding materials are popular for their use in various fields such as electricity production, military surveillance, and research activities.[8,9] Thermoluminescence (TL) is the most basic characteristic of radiation dose materials. Borate glass has excellent thermoluminescence properties, and has better transparency, mechanical strength, and chemical durability.[10,11] Therefore, it is a high-performance shielding material that is expected to replace concrete. Potassium-ion batteries (PIBs) have advantages such as abundant reserves, low cost, and oxidation–reduction potentials similar to those of lithium-ion batteries (LIBs), making them preferred alternatives to LIBs.[12] The introduction of potassium ions into borate glass helps to improve the strength and electron emission capacity of this glass.[13] In terms of bioactive amorphous materials, the addition of K_2O enhances ion diffusion rates to promote bone formation.[14] The abnormal properties of potassium borate glass depend on its structure, and the diversity of structural units and the variability of K–O and B–O coordination numbers bring challenges to its structural analysis.

A variety of techniques have been used to study the complex structures of borate glass. Raman spectroscopy indicates that the main structural units present in potassium borate glass include metaborate units, pyroborate units, orthoborate units, boroxol rings, di-borate groups and tetraborate groups.[15–19] ^{11}B NMR experimental results and physical–chemical models suggest that the peak value of N_4 occurs at $x = 0.30$.[19,20] Wright *et al.*[21] used neutron diffraction to determine the distance of the first coordination shell of B–O interactions in the $0.28K_2O{\cdot}0.72^{11}B_2O_3$ glass structure as being ~1.4 Å, with $r_{B\text{–}O(B\varnothing 3)}$ = 1.38 Å and $r_{B\text{–}O(B\varnothing 4^-)}$ = 1.46 Å. Handa *et al.*[22] reported that the B–O, K–O and O–O bond lengths in $0.20K_2O{\cdot}0.80^{11}B_2O_3$ glass are 1.39, 2.83 and 2.40 Å, respect-

[a]*Key Laboratory of Green and High-end Utilization of Salt Lake Resources, Qinghai Institute of Salt Lakes, Chinese Academy of Sciences, Xining 810008, China. E-mail: zhufayan@126.com*
[b]*University of Chinese Academy of Science, Beijing 100049, China*
[c]*ISIS Facility Rutherford Appleton Laboratory, Chilton, Didcot, Oxon OX11 0QX, UK*
[d]*Coe College, Physics Department, 1220 First Ave NE, Cedar Rapids, IA 52402, USA*
†Electronic supplementary information (ESI) available. See DOI: https://doi.org/10.1039/d4dt00804a

ively. At higher $B\varnothing_4^-$/NBO ratios, alkali and alkaline earth metal cations primarily act as "network formers", while at higher NBO contents, they primarily act as "network modifiers".[23–26] Furthermore, at higher NBO contents, the main oxygen atoms in $B\varnothing_4^-$ units are also NBOs.[23] An increase in $B\varnothing_4^-$ content in this glass helps to enhance its thermal and mechanical stability, while an increase in NBO results in denser glass,[27] because the B–NBO bond is longer than the B–BO bond.[28] In zinc borate glass, the density increases and the molar volume decreases with increasing ZnO content.[29] In lithium borate glass, the density initially increases and then decreases, while the molar volume decreases with increasing Li_2O content.[30] The arrangement of network modifier atoms in uniformly nucleated glass structures is close to that in crystals of a similar component.[31,32] The study of metallic glass also shows that the medium range structure exists in both glass and crystal,[33] and the medium range structure is closely related to magnetic order.[34] The above literature shows that the short and medium-range ordered structure is the key structure of glass, which is crucial for the regulation of microscopic properties. At present, the ion-transport mechanism of potassium borate glass as a solid electrolyte remains to be explored, and there is a lack of relevant studies into the effect of short- and medium-range structural changes on the amorphous properties, especially the internal relationship between NBO, $B\varnothing_4^-$ and density, ion transport and other properties, which are still unclear.

In this work, neutron diffraction experimental data are analyzed using EPSR and difference subtraction methods, and structure information on potassium borate glass is obtained. Meanwhile, the molecular dynamics simulation method is used to supplement the verification. The effect of glass structure on ion transport, density and molar volume is discussed based on obtaining the structure information of atomic interaction distance and coordination number, ring and chain structure unit, micro-cavity distribution and NBO content change. This study provides a reference for revealing the influence of the medium- and short-range structure on amorphous properties.

2. Experimental

2.1. Sample preparation and characterization

Using isotopic boric acid of analytical purity (purity: 99.27%, company: Eagle-Picher) and potassium carbonate of analytical purity (purity: 99.0%) as raw materials, they were thoroughly mixed in a platinum crucible and then heated in a muffle furnace at 1000 °C for 15 minutes. The temperature was raised to 1100 °C and heating continued for 10 minutes. Colorless, transparent, and uniform potassium borate glass samples with composition $x{K_2O}\cdot(1-x)^{11}B_2O_3$ (x = 0.10, 0.20, 0.30, and 0.40) were prepared by the quenching method on a flat plate. As potassium borate glass is highly hygroscopic, the prepared samples were first sealed and then stored in a nitrogen atmosphere glove box.

The composition, mass density (ρ_n), atomic density (ρ_a), and molar volume (V_m) of potassium borate glass are shown in Table 1. The deviation of sample composition caused by mass loss is within ±0.016. For calculations formulas of atomic density and molar volume, and for the conversion formula of isotopic sample density to natural boron sample density, please refer to our previous work.[30]

2.2. Neutron diffraction

Neutron diffraction experiments on potassium borate glass were conducted on the GEM diffractometer at the ISIS Spallation Neutron Source (Rutherford Appleton Laboratory)[35] in the UK. The experiments were carried out in a vacuum-sealed vanadium can at room temperature (inner diameter 8.3 mm, wall thickness 25 μm) in an attempt to reduce contact between the sample and air, considering that the potassium borate glass sample is prone to moisture absorption and deterioration during the experiment. The standard ATLAS program[36] was used to correct the data from detector groups 1, 2, 3, 4, and 5 (covering a 2θ range from 5.32° to 107.07°) for background diffraction and container diffraction, multiple diffraction, self-attenuation and inelastic (Placzek) effects to obtain a distinct scattering function $i(Q)$. The neutron diffraction data of the measured vanadium niobium rod were used for data normalization. The $i(Q)$ data were subjected to Fourier transformation and Lorch correction[37] to obtain the total correlation function $T(r)$. The relevant calculation equations follow,[38,39] where the distinct scattering $i(Q)$ is given by the following equation:

$$i(Q) = \sum_{l,l'} \bar{b}_l \bar{b}_{l'} \sum_{\substack{j=1 \\ j \neq k}}^{N_l} \sum_{k=1}^{N_{l'}} \frac{1}{N} \frac{\sin(QR_{jk})}{QR_{jk}} \quad (1)$$

Structural information may then be obtained by Fourier transformation of $i(Q)$, yielding the total correlation function

$$T'(r) = T^0(r) + \frac{2}{\pi}\int_0^\infty Qi(Q)M(Q)\sin(rQ)\mathrm{d}Q \quad (2)$$

Table 1 The composition, mass density, atomic density and molar volume of potassium borate glass

Sample	Nominal composition		Composition from mass loss		ρ_n (iso) (g cm^{-3})	ρ_n (nat) (g cm^{-3})	ρ_a (Å^{-3})	V_m (mol cm^{-3})
	K_2O (x)	$^{11}B_2O_3$	K_2O	$^{11}B_2O_3$				
$0.10K_2O\cdot0.90^{11}B_2O_3$	0.1000	0.9000	0.0925	0.9075	2.0200	2.0102	0.0843	35.7310
$0.20K_2O\cdot0.80^{11}B_2O_3$	0.2000	0.8000	0.1958	0.8042	2.1303	2.1211	0.0868	34.7531
$0.30K_2O\cdot0.70^{11}B_2O_3$	0.3000	0.7000	0.2879	0.7121	2.2644	2.2556	0.0900	33.3799
$0.40K_2O\cdot0.60^{11}B_2O_3$	0.4000	0.6000	0.3840	0.6160	2.2788	2.2707	0.0893	33.7523

where $M(Q)$ is a modification function. The average density contribution to the correlation function is

$$T^0(r) = 4\pi r g^0 \left(\sum_l c_l \overline{b_l} \right) \quad (3)$$

The correlation function is a weighted sum of partial correlation functions, $t_{ll'}(r)$

$$T(r) = \sum_{l,l'}^{l \geq l'} c_l (2 - \delta_{ll'}) \overline{b_l b_{l'}} t_{l-l'}(r) \quad (4)$$

where the l,l' summations are over all unique pairs of elements in the sample.

2.3. Molecular dynamics simulation

Born–Oppenheimer molecular dynamics simulation of the potassium borate glass structure was carried out using the CP2K program.[40] The generalized gradient approximation and the PBE function were applied.[41] The initial atomic configuration of vitreous potassium borate was generated using packmol.[42] The cubic simulation box at room temperature contains approximately 400 atoms (depending on the composition of each sample, as shown in Table S1†) to match the experimental number density. Further optimization is performed using density functional theory (DFT), and the molecularly optimized consistent polarization double-zeta basis set DZVP[43] and Goedecker–Teter–Hutter (GTH) type pseudopotentials[44] are adopted for each atom involved. The FPMD simulation after DFT optimization starts at 298.15 K. A Nosé–Hoover heat bath[45,46] with a length of 3 is used in a typical NVT ensemble. The samples are heated from 298.15 K to above the glass transition temperature (~925 K) to 1398.15 K with a gradient of 400 K, a time step of 1 fs per step, and for 10–20 ps at each temperature. At 1398.15 K, the system is balanced for 20 ps, and it is then cooled to 298.15 K following the same temperature step and similar simulation time values. Finally, after being balanced for 20 ps at 298.15 K, the data are collected. The connectivity and distribution of the ring structure were analyzed using R.I.N.G.S.[47] Pore distribution analysis was carried out using the pyMolDyn[48] program. The Visual Molecular Dynamics (VMD)[49] program was used to analyze the simulated trajectories and visualize them graphically. The ion-transport path of K^+ in glass was studied by applying an electric field of 0.02 a.u. along the Z-axis and fixing the boron–oxygen network structure.

2.4. Empirical potential structure refinement

The empirical potential structure refinement (EPSR) method[50] was used to analyze the neutron diffraction experimental data of potassium borate glass. The model uses reference potentials consisting of standard Lennard-Jones plus Coulomb terms. When building the model, approximately 4500 atoms (K, B, O atoms) are placed in a cubic box with periodic boundary conditions. The Lennard-Jones potential parameters, the atomic charges, box composition and box size are listed in Tables S2 and S3.† Before the empirical potential structure refinement, the model is subjected to a continuous NVT Monte Carlo equilibrium under the reference potential after running to equilibrium at 10 000 K, and the initial structural model is obtained through a continuous cooling process at 1400 K, 1200 K, 1000 K, 700 K, and 300 K. Then the relaxation balance is performed by adjusting the appropriate ereq value, and the potassium borate glass structure model and smooth pdf data are obtained.

3. Structure and discussion

3.1. Neutron diffraction data

The interference function of potassium borate glass is shown on the left of Fig. 1. As can be seen from the figure, the oscillation amplitude of the $i(Q)$ data at high Q is very small and the data are smooth, indicating that the neutron diffraction data of potassium borate glass obtained in this study are of high quality. There are three peaks, Q_0, Q_1, and Q_2, when $0 < Q < 3.7$ Å^{-1}. Q_0 is related to the K–K interaction. With the increase of K_2O content, the corresponding atomic interaction distance decreases (5.61 Å to 5.07 Å), the atomic interaction range indicated by Q_1 and Q_2 increases, and the short- and medium-range ordered structure increases. The total correlation function of potassium borate glass is shown on the right of Fig. 1. As can be seen from the figure, there are three main interaction peaks, P_1, P_2, and P_3, within the range of 4 Å. The P_1 peak represents the B–O interaction. As the content of K_2O increases, the intensity of the P_1 peak decreases, the half-peak width increases, and the r value increases from 1.38 to 1.41 Å. The P_2 peak includes four types of interaction: B–B, O–O, B–O, and K–O. The P_3 peak contains four types of interaction: B–O, O–O, K–K, and K–B. As the content of K_2O increases, the intensity of both P_2 and P_3 peaks decreases, full-width at half maximum (FWHM) increases, and the corresponding r values increase from 2.39 to 2.42 Å, and 3.63 to 3.68 Å, respectively.

3.2. Analysis of neutron experiment data

3.2.1. The difference method. The potassium borate glass $T(r)$ spectrum is very complicated, especially the P_2 and P_3 peaks. Taking $0.1K_2O{\cdot}0.9^{11}B_2O_3$ glass as an example, the first peak in the $T(r)$ spectrum has good symmetry and only contains the B–O interaction.[51] As shown in the left-hand graphs of Fig. 2, the B–O interaction in the P_2 peak is simulated based on the second coordination shell B–O distance (2.79 Å) in the $g_{B-O}(r)$ of the AIMD simulation data, and its coordination number and root-mean-square deviation $\langle u_{BO}{}^2 \rangle^{1/2}$ references the neutron and X-ray diffraction data of B_2O_3 glass.[52,53] The distance and coordination number of the O–O interaction are based on the first coordination shell O–O interaction information in the $g_{O-O}(r)$ of the AIMD simulation data. By subtracting the simulated $T(r)_{B-O,\ O-O}$(simu) from the total $T(r)$exp data, the differential data $T(r)_{B-B,\ K-O}$(diff) containing only B–B and K–O interactions, and then the B–B and K–O interactions, can be obtained by fitting. The analysis of the P_3 peak also

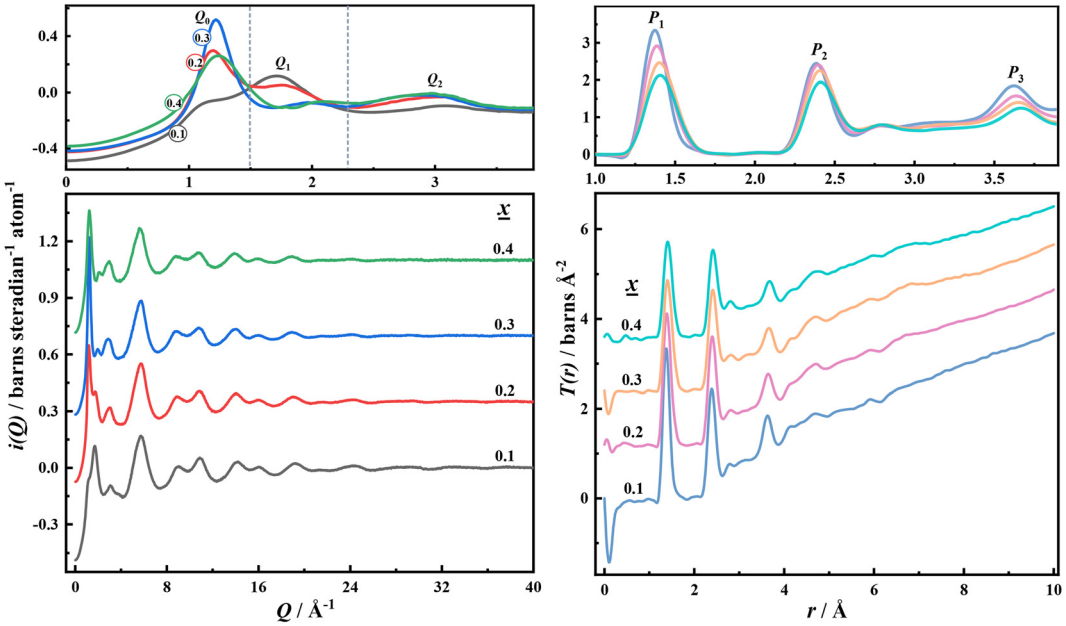

Fig. 1 Left panel: Interference function $i(Q)$ of potassium borate glass and right panel: total correlation function $T(r)$ of potassium borate glass.

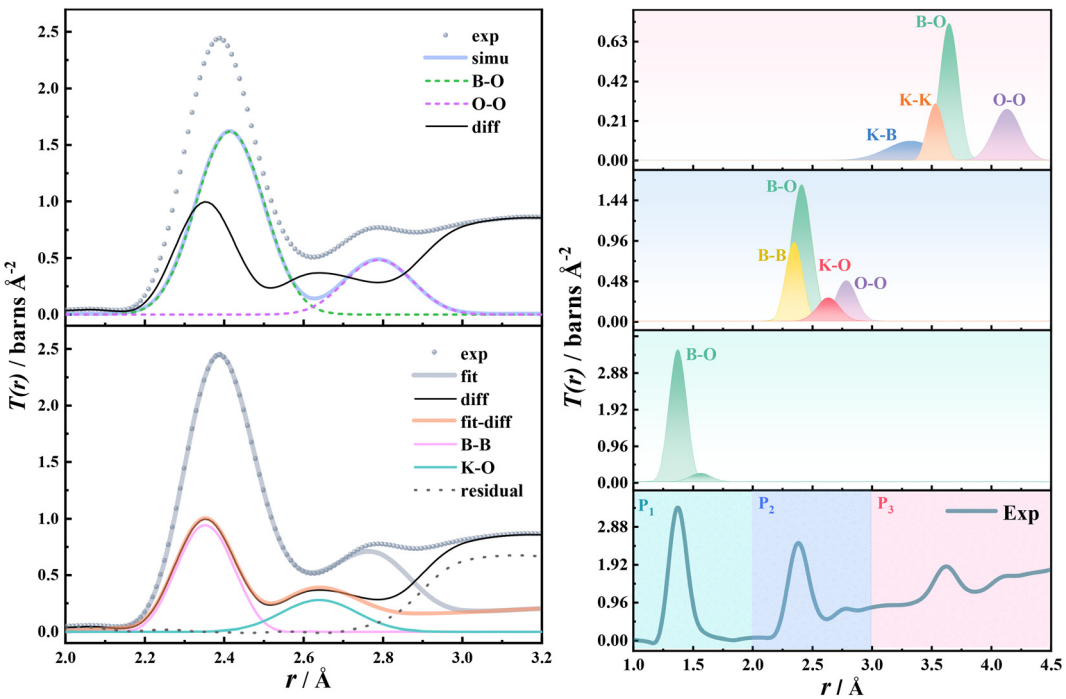

Fig. 2 Real spatial distribution function $T(r)$ of $0.1K_2O{\cdot}0.9^{11}B_2O_3$ glass. Left panel: the fitting of peak P_2, where the top figure shows the simulated B–O and O–O peaks, while the lower figure shows the B–B and K–O peaks obtained by subtraction. Right panel: the fitted peaks P_1, P_2 and P_3.

adopts the difference method, and the simulation of B–O, O–O and K–B interactions refers to the AIMD simulation results and B_2O_3 glass data,[52,53] which are similar to the results of the analysis process of the P_2 peak, as shown in the right-hand graphs of Fig. 2. The information of atomic pair interaction distance and coordination number in $xK_2O{\cdot}(1-x)^{11}B_2O_3$ (x = 0.10, 0.20, 0.30, and 0.40) glass is shown in Table S4.† As can be seen from the table, with the increase of K_2O content, the B–O distance increases from 1.37 to 1.41 Å, and the O–O action distance changes little. In summary, the B–O distance increases with the increase of K_2O content in potassium borate glass, and bond $r_{B-O}(B\varnothing_4^-)$ = 1.46 Å grows larger than that of $r_{B-O}(B\varnothing_3)$ = 1.38 Å,[19] so the increase of B–O distance is closely related to the increase of $B\varnothing_4^-$ content. However, the

maximum point of the $B\varnothing_4^-$ content is x = 0.3,[20] indicating that there are other factors affecting the B–O bond length besides the $B\varnothing_4^-$ content, which will be discussed further later.

3.2.2. Analysis of PDF data obtained by EPSR and AIMD methods. The $F(Q)$ and $G(r)$ spectra of the experiment on and EPSR simulation of potassium borate glass are shown in Fig. S1 (ESI).† It can be seen from the figure that the EPSR simulation $F(Q)$ and $G(r)$ data overlap well with the neutron experiment data, indicating that the EPSR simulation better presents the experimental data.

B–O interactions. The pair distribution function (PDF) of B–O interactions and B–O bond lengths in different structural units obtained by the EPSR and AIMD methods are shown in Fig. 3. As shown in the figure, the PDF data obtained by the two methods differ slightly, mainly due to the different calculation principles of the two methods[40,50] and the box sizes (Tables S1 and S3†). The B–O interaction distances of xK$_2$O·$(1-x)^{11}$B$_2$O$_3$ ($0.1 \le x \le 0.4$) glass from experimental data are 1.37, 1.39, 1.40, and 1.41 Å, respectively, which are close to the results obtained by the AIMD, EPSR and subtraction methods (Table S4†). In addition, the B–O interaction distance increases with the increase of K$_2$O content. The coordination number distribution of the B–O interaction is shown in Fig. S2.† It can be seen from the figure that with the increase of K$_2$O content, the B–O coordination number gradually increases, which is consistent with the changing trend of the B–O coordination number obtained by the difference method (Table S4†). The maximum point of the change of the tetra-coordinated boron content (N_4) is located at x = 0.30, accounting for about 30%,[20] indicating that the coordination number of the B–O interaction is less than 3.5, which is close to the results of the B–O coordination number given in this paper. According to the research results given by Koroleva *et al.*,[20] the main basic structural units in potassium borate glass are $B\varnothing_3$ and $B\varnothing_4^-$ when x = 0.1 and 0.2. At x = 0.3, the $B\varnothing_2O^{2-}$ structural unit begins to appear, and at x = 0.4, the $B\varnothing_2O^{2-}$ becomes the main structural unit and the $B\varnothing O_2^{2-}$ structural unit begins to appear. Therefore, the B–O effect in potassium borate glass is mainly that of tri-coordination, but with the increase of K$_2$O content, the proportion of NBO in tri-coordinated boron also increases, and the change of the overall basic structural unit in the glass is that the content of $B\varnothing_3$ decreases, the content of $B\varnothing_4^-$ increases, and the content of $B\varnothing_{(3-a)}O_a^{a-}$ (a = 1 or 2) increases. The change in the basic structural unit causes the three-dimensional connectivity of the glass to increase and the boron–oxygen network structure to become dispersed, so the density of the glass increases (Fig. S3†).

In this work, the atom labeling method was used to mark ^{3}B, ^{4}B, BO, and NBO atoms in the equilibrium structure simulated by AIMD, respectively. Then four kinds of B–O interactions of ^{3}B–BO, ^{3}B–NBO, ^{4}B–BO, and ^{4}B–NBO were obtained. At the same time, the $K_2B_4O_7$ crystal containing ^{3}B and ^{4}B (the mole content of K$_2$O is 0.33) and the $K_3B_3O_6$ crystal containing BO and NBO (the mole content of K$_2$O is 0.50) were also marked in the same way, as shown in Fig. 4, with the related data being shown in Table S5.† As can be seen from the figure, there are obvious differences between the structures of the glass and the crystals with similar components: (1) there is a small proportion of ^{4}B–NBO interactions in the $0.40K_2O{\cdot}0.60^{11}B_2O_3$ glass, at about 2.6%, while there is no such interaction in other glasses; (2) the main B–O interaction in the $0.40K_2O{\cdot}0.60^{11}B_2O_3$ glass is ^{3}B–BO, at about 57.3%, whereas the ^{4}B–BO interaction is at about 23.5%, while the proportions of ^{3}B–BO and ^{4}B–BO interactions in the $K_2B_4O_7$ crystal are very close; (3) the bond lengths of ^{3}B–BO in $0.40K_2O{\cdot}0.60^{11}B_2O_3$ glass, $K_2B_4O_7$, and $K_3B_3O_6$ crystals are 1.40, 1.37, and 1.37 Å, respectively. The ^{4}B–BO and ^{3}B–NBO bond lengths (1.49 and 1.35 Å) in the glass are longer than those (1.48, 1.33 Å) in the crystal. In addition, the B–O bond length in the $K_2B_4O_7$ crystal (1.42 Å) is much longer than the

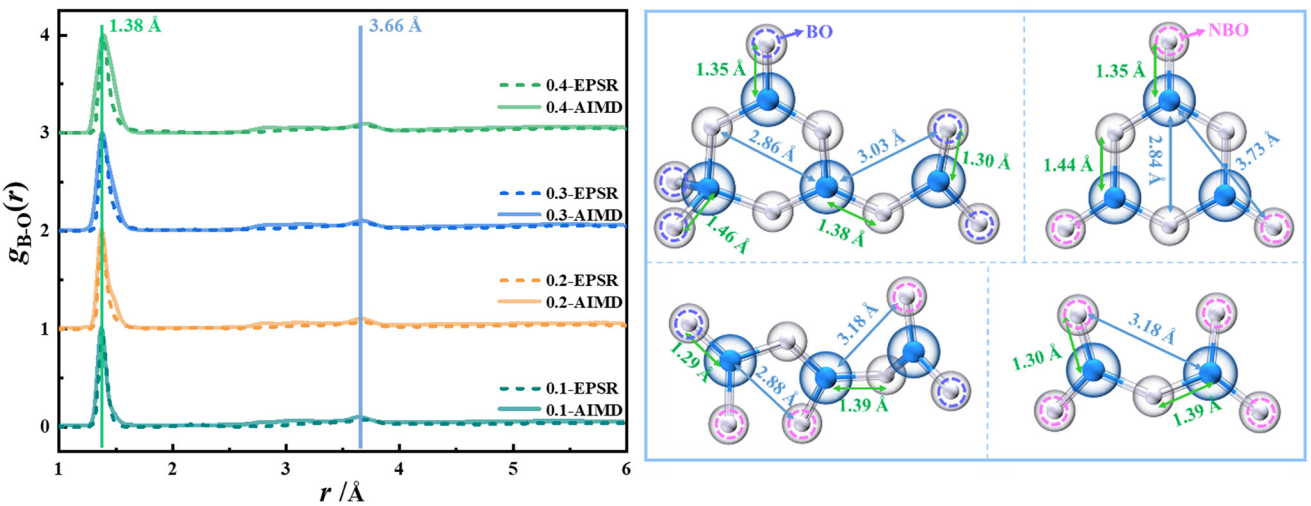

Fig. 3 Pair distribution function of B–O interactions and B–O bond lengths in different structural units in xK$_2$O·$(1-x)^{11}$B$_2$O$_3$ ($0.1 \le x \le 0.4$) glass obtained by EPSR and AIMD methods.

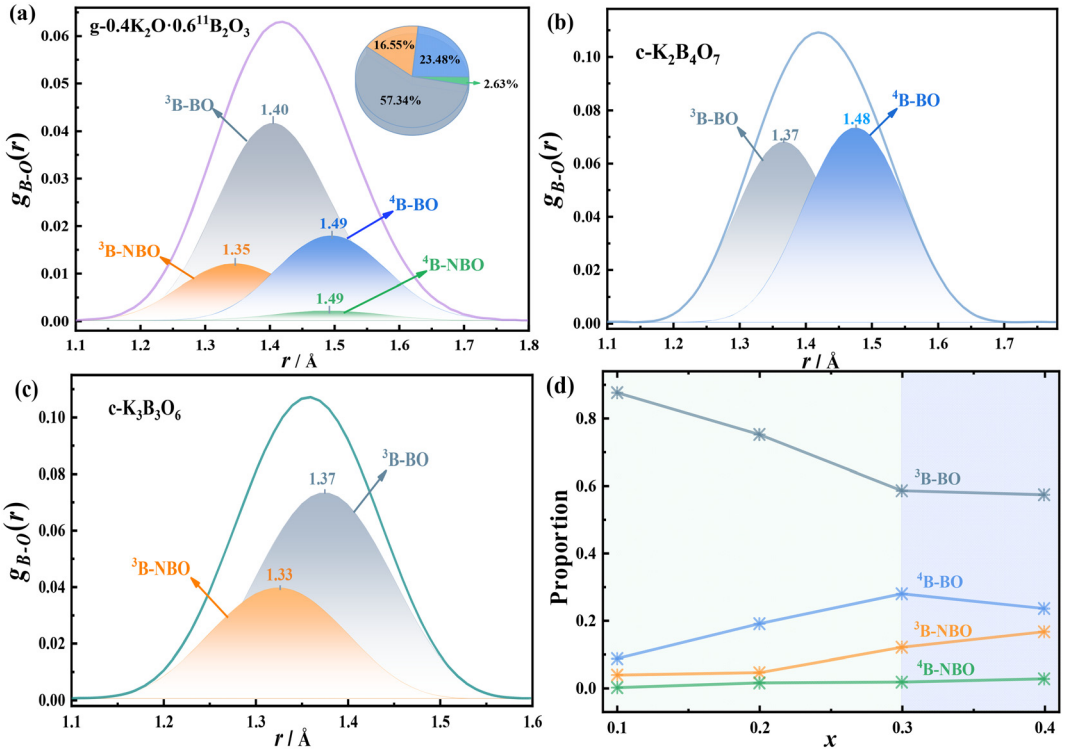

Fig. 4 (a), (b) and (c) represent the distribution of ^{3}B–BO, ^{3}B–NBO, ^{4}B–BO and ^{4}B–NBO interactions in the first coordination layer of the B–O interaction in $0.40K_2O{\cdot}0.60^{11}B_2O_3$ glass and $K_2B_4O_7$ and $K_3B_3O_6$ crystals, respectively. The inset pie chart in the panel for $0.40K_2O{\cdot}0.60^{11}B_2O_3$ glass shows the percentages of each atom-pair interaction. (d). The relative contents of the ^{3}B–BO, ^{3}B–NBO, ^{4}B–BO and ^{4}B–NBO interactions in $xK_2O{\cdot}(1-x)^{11}B_2O_3$ ($0.1 \le x \le 0.4$) glass.

B–O bond length in the $K_3B_3O_6$ crystal (1.36 Å). The above information shows that potassium borate glass contains more B–O bond types than crystals with similar components, and the bond lengths of ^{3}B–BO, ^{4}B–BO and ^{3}B–NBO are longer than those of corresponding crystals, indicating that the boron–oxygen network of glass is looser than that of similar-component crystals. Fig. S3† shows that the density of the glass is smaller than that of the crystals of similar components, confirming the conclusion that the structure of the glass is relatively loose. In both glass and crystal, the increase of NBO decreases the length of the B–O bond, and the increase of ^{4}B increases the length of the B–O bond. In addition, Edén *et al.*'s study[23] concluded that the bond lengths of ^{3}B–NBO, ^{3}B–BO, ^{4}B–NBO and ^{4}B–BO in sodium borate glass are 1.34, 1.35, 1.34 and 1.43 Å, respectively, and the bond lengths all increase gradually with the increase of Na_2O content. Obviously, the four B–O interactions in the structure of potassium borate glass are at greater distances than the corresponding atomic pairs in sodium borate glass, indicating that the arrangement of B and O atoms in potassium borate glass is looser, which is also the structural reason why the density of potassium borate glass is less than that of sodium borate glass.[54]

The relative contents of the ^{3}B–BO, ^{3}B–NBO, ^{4}B–BO and ^{4}B–NBO interactions in $xK_2O{\cdot}(1-x)^{11}B_2O_3$ ($0.10 \le x \le 0.40$) glass are shown in Fig. 4(d), where $x = 0.30$ is the inflection point of the four interaction changes, which is also the maximum point of the tetra-coordinated boron (^{4}B) content.[15,17,19] As can be seen from the figure, ^{3}B–BO has the highest relative content, followed by ^{4}B–BO and ^{3}B–NBO. When $0.10 \le x \le 0.30$, with the increase of K_2O content, the ^{3}B–BO interaction significantly decreases, the ^{3}B–NBO and ^{4}B–BO interactions increase, and the total B–O bond length increases. When $0.30 \le x \le 0.40$, the ^{3}B–BO interaction changes little, the ^{4}B–BO interaction decreases, the ^{3}B–NBO interaction increases, the ^{4}B content decreases slightly, but a new ^{4}B–NBO interaction is generated, so the total B–O bond length still increases. The maximum point for the content of $B\varnothing_4^-$ ($x = 0.3$) is also the maximum point of density and atomic density, and the minimum point of the molar volume of potassium borate glass (Fig. S3†). On the one hand, due to the increase of $B\varnothing_4^-$ content, the boron–oxygen network connectivity is enhanced, the atomic arrangement of the glass becomes denser, and the corresponding molar volume decreases. On the other hand, the increase of NBO content (Fig. S4†) and the length of the B–NBO bond being shorter than the B–BO bond leads to the shortening of the distance between B and O atoms in the boron–oxygen network structure, the increase of glass density and the decrease of molar volume. Thus, the effects of $B\varnothing_4^-$ and NBO on properties are synergistic rather than independent.

O–O interactions. The pair distribution function of the O–O interactions in the structure of potassium borate glass is shown in the upper panel of Fig. 5. As can be seen from the

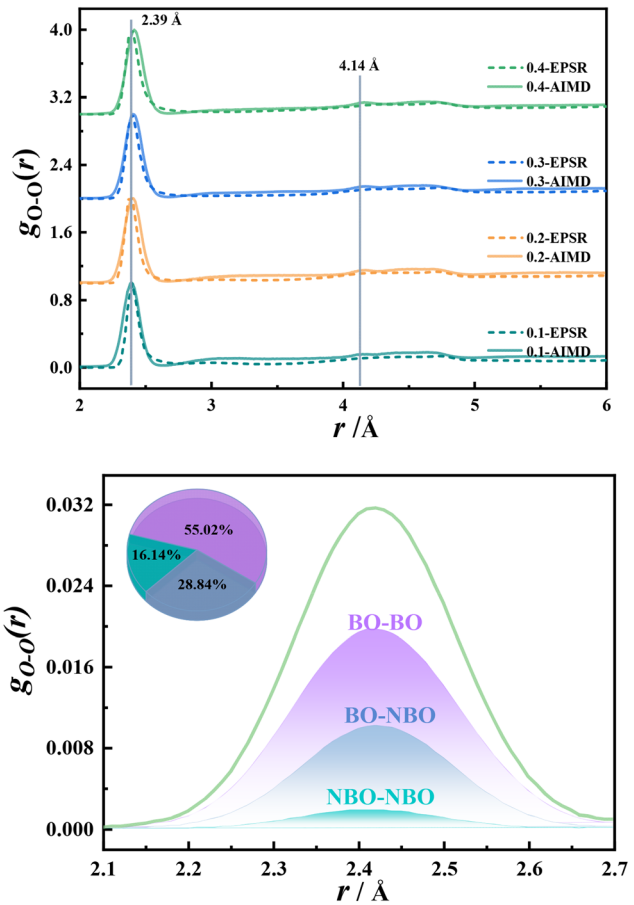

Fig. 5 Upper panel: Pair distribution function of the O–O interaction in xK$_2$O·(1 − x)^{11}B$_2$O$_3$ (0.1 ≤ x ≤ 0.4) glass obtained by EPSR and AIMD methods. Lower panel: PDF diagram of BO–BO, BO–NBO and NBO–NBO interactions in the first coordination layer of the O–O interaction in 0.40K$_2$O·0.60^{11}B$_2$O$_3$ glass.

figure, with the increase of K$_2$O content, the distance of the first coordination shell of O–O interactions increases from 2.40 to 2.42 Å, indicating that the addition of K$_2$O elongates the O–O distance. The research of Handa *et al.*[22] also supports this conclusion. However, the reason for the increasing O–O distance is still unclear. In this work, the atomic labeling method is used to denote three types of O–O interactions: BO–BO, BO–NBO, and NBO–NBO, as shown in the lower panel of Fig. 5. In 0.40K$_2$O·0.60^{11}B$_2$O$_3$ glass, the proportion of BO–BO interactions is the highest, accounting for about 55.02%, followed by that of BO–NBO and NBO–NBO, accounting for 28.84% and 16.14%, respectively. It is worth noting that the distances of the three types of O–O interactions are basically the same, all located at 2.42 Å. This indicates that there is little correlation between the content of NBO and the O–O distance. In K$_2$B$_4$O$_7$ crystals containing B$\varnothing_4^-$ and BO$_3$, the O–O distance in B$\varnothing_4^-$ is about 2.43 Å, and the O–O distance in BO$_3$ is about 2.37 Å, indicating that the increase in the O–O distance in the glass is related to B$\varnothing_4^-$. In summary, with the increase of K$_2$O content in potassium borate glass, the B$\varnothing_4^-$ content gradually increases, although the O–B–O bond angle decreases (Fig. S5†), and the ^{4}B–O bond distance still increases, so the O–O distance increases. Therefore, the density increase of potassium borate glass is mainly related to the content of NBO and B$\varnothing_4^-$, and has no direct correlation with the O–O effect.

K–O interaction. The first coordination layer distance of K–O interaction in xK$_2$O·(1 − x)^{11}B$_2$O$_3$ (0.1 ≤ x ≤ 0.4) glass is 2.835, 2.815, 2.735 and 2.715 Å, respectively, and the K–O distance decreases gradually with the increase of K$_2$O content. The interaction between K–BO and K–NBO was obtained by the atomic labeling method. Fig. 6(a) shows the PDF diagram of the first coordination layer of K–O interaction. It can be seen from the diagram that the relative proportions of K–BO and K–NBO interaction are very close, at 50.99% and 49.01%, respectively, with bond lengths of 2.80 and 2.71 Å. This suggests that K$^+$ and NBO form a stronger bond. However, the distance between K–BO and K–NBO in potassium borate crystals with similar components is close, as shown in Fig. 6(b). Fig. 6(c) shows the variation of the K–BO and K–NBO interactions in xK$_2$O·(1 − x)^{11}B$_2$O$_3$ (0.1 ≤ x ≤ 0.4) glass. As the content of K$_2$O increases, the proportion of K–BO interactions gradually decreases, while the proportion of K–NBO interactions gradually increases. The turning point is x = 0.20. This point also happens to be the maximum point of the K–O coordination number, as shown in Fig. S2.† When x = 0.40, the numbers of K–BO and K–NBO interactions are very close. The structure image in Fig. 6 shows snapshots of 0.10K$_2$O·0.90^{11}B$_2$O$_3$ and 0.40K$_2$O·0.60^{11}B$_2$O$_3$ glass when K$^+$ is 8-coordinated. In 0.10K$_2$O·0.9011B$_2$O$_3$ glass, K$^+$ mainly coordinates with BO. As K–NBO interaction increases, in the 0.40K$_2$O·0.60^{11}B$_2$O$_3$ glass, K$^+$ coordinates with four NBOs and four BOs. Therefore, as the content of K$_2$O increases, the content of NBO increased, and the structural units containing NBO increased, so the interaction of K$^+$ with NBO increases. In lithium borate glass, when the content of NBO also increases with the increase of Li$_2$O content,[55] the results show that both Li$_2$O and K$_2$O will destroy the ring structure of B$_2$O$_3$ glass and gradually transform it into a "molecular" structural unit containing NBO. Kamitsos *et al.*'s[56] study of the far infrared spectral region of K$_2$O·2B$_2$O$_3$ glass show that potassium ions exist in two vibration modes: L bands (low frequency) and H bands (high frequency). Combined with the research of Bray *et al.*,[57] the H bands may correspond to the vibration associated with K–NBO, while the L bands correspond to the vibration associated with K–BO. When x = 0.33, in our work, the relative content of K–NBO is about 0.41, while the results from Kamitsos *et al.*[56] reveal that it is about 0.57 ± 0.05. This difference is mainly caused by the error of different research methods.

3.2.3. Structure analysis of rings and cavities. The ring distribution of xK$_2$O·(1 − x)^{11}B$_2$O$_3$ (x = 0.10, 0.20, 0.30, and 0.40) glass is shown in Fig. 7. As seen from the figure, potassium borate glass contains numerous four-membered ring, six-membered ring, eight-membered ring, ten-membered ring, and twelve-membered ring structures. When 0.10 ≤ x ≤ 0.30, initially, a structural transformation mainly occurs from a boroxol ring to a six-membered ring containing B$\varnothing_4^-$, as shown in Fig. S7.† With the increase of K$_2$O content, the six-

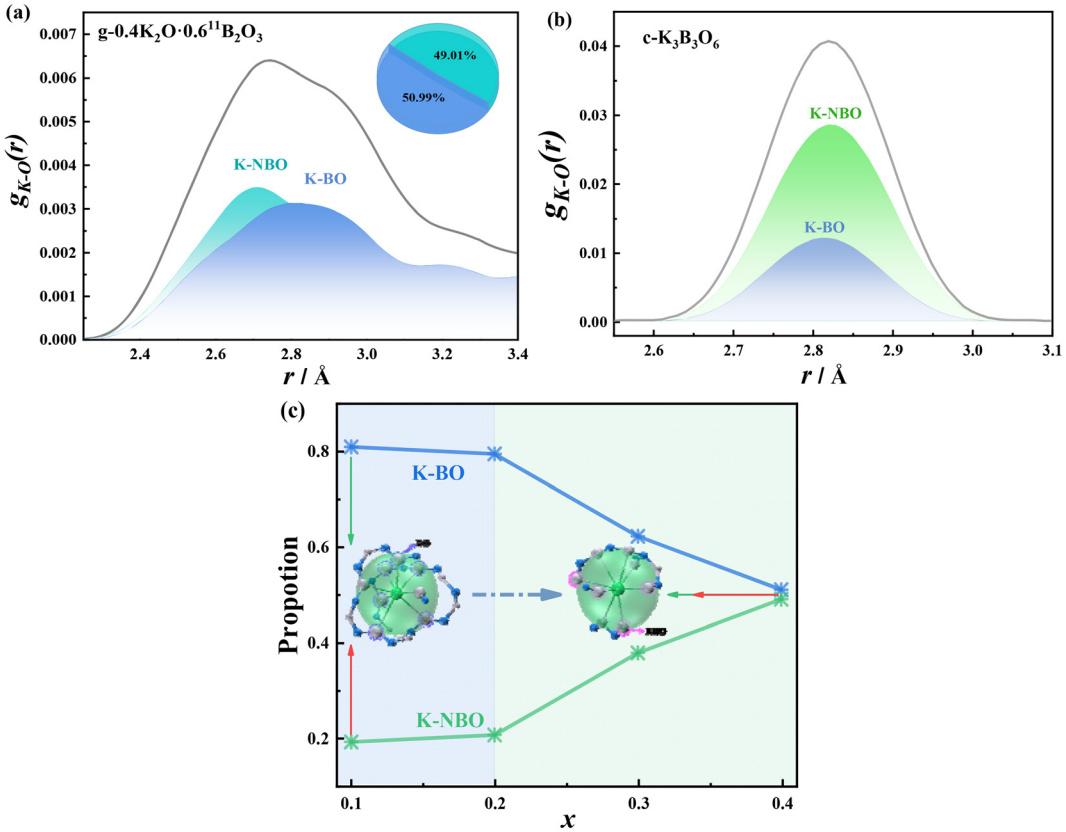

Fig. 6 (a) The distribution of K–BO and K–NBO interactions in the first coordination layer of the K–O interaction in $0.40K_2O{\cdot}0.60^{11}B_2O_3$ glass. The pie chart on the right shows the percentages of each atom-pair interaction. (b) The distribution of K–BO and K–NBO interactions in the first coordination layer of the K–O interaction in the $K_3B_3O_6$ crystal. (c) Changes in the relative contents of K–BO and K–NBO interactions in $xK_2O{\cdot}(1-x)^{11}B_2O_3$ ($0.1 \le x \le 0.4$) glass.

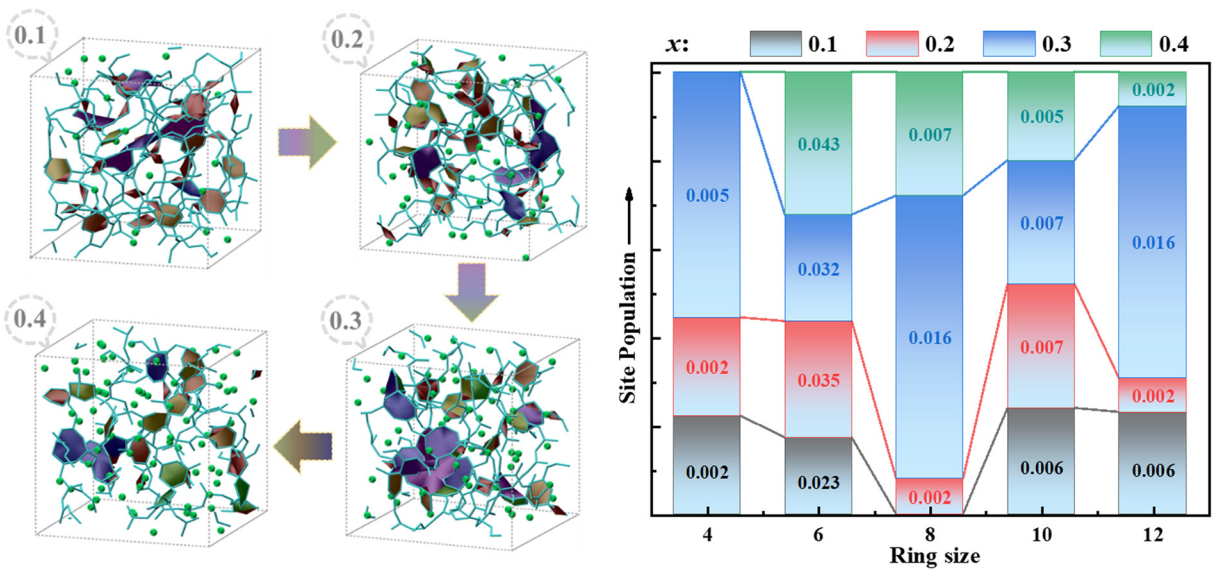

Fig. 7 Rings and ring-size distribution in a simulated box of $xK_2O{\cdot}(1-x)^{11}B_2O_3$ ($0.1 \le x \le 0.4$) obtained by AIMD methods.

membered ring containing one $B\varnothing_4^-$ is further transformed into a six-membered ring containing two $B\varnothing_4^-$ tetrahedra (Fig. S7†), and the conversion process from the boroxol ring to the diborate unit and the eight-membered ring occurs, as shown in Fig. 8. Finally, most ring structures are connected by sharing the B–O bond, resulting in a large-ring reunion, as

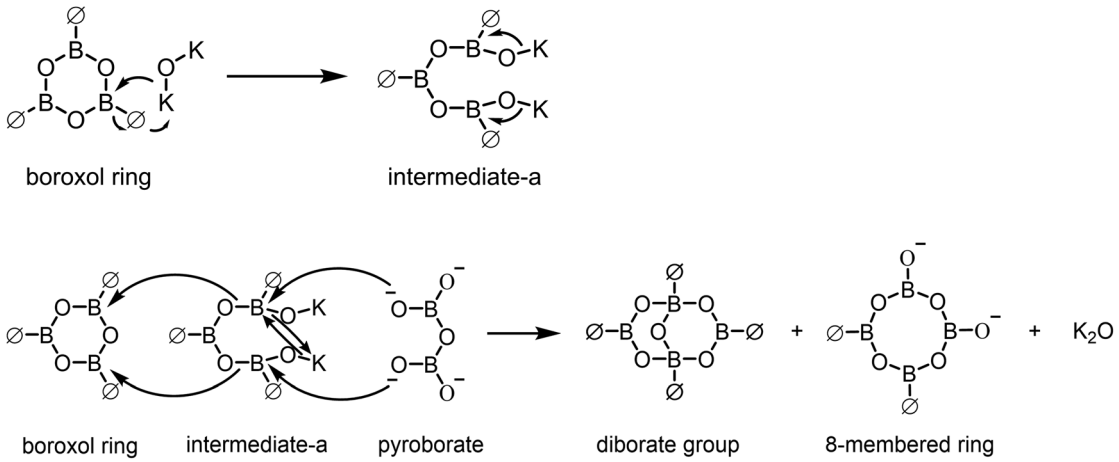

Fig. 8 Schematic diagram of the conversion mechanism between the boroxol ring and the diborate group, 8-membered ring.

shown in Fig. S6,† of three six-membered rings. When $0.30 < x \leq 0.40$, the large ring structures decrease significantly, and the six-membered rings increase obviously. Moreover, metaborate chains and rings, and pyroborate units began to appear, which include more NBO. The agglomeration phenomenon of the ring structure disappeared, and the ring structure was evenly dispersed over the whole system. Raman spectroscopy experimental results also show that when $x = 0.40$, the metaborate chains increase obviously and the ring structure depolymerizes.[20] The right-hand panel of Fig. 7 shows the ring size distribution of $x{}^{11}K_2O{\cdot}(1-x){}^{11}B_2O_3$ (x = 0.10, 0.20, 0.30, and 0.40) glass. As seen from the figure, the system with the lowest number of rings is $0.1{}^{11}K_2O{\cdot}0.9{}^{11}B_2O_3$ glass. The system with the largest number of rings is $0.3{}^{11}K_2O{\cdot}0.7{}^{11}B_2O_3$ glass, wherein the six-membered rings are the most numerous, accounting for about 51% of the total number of rings. The system with the most six-membered rings is $0.4{}^{11}K_2O{\cdot}0.6{}^{11}B_2O_3$ glass, accounting for 75% of the total number of rings. Therefore, the increase in the K_2O content causes the ring structure in the potassium borate glass to first increase and then decrease, with the turning point being $x = 0.3$. When $x = 0.3$, the tetra-coordinated boron content is the highest, resulting in the strongest network connectivity and the largest number of rings.[19,20] When $x > 0.3$, the ring structure depolymerizes, the content of large rings decreases, the content of six-membered rings increases, and the ring structure becomes evenly dispersed.

The distribution of cavities of $x{}^{11}K_2O{\cdot}(1-x){}^{11}B_2O_3$ glass obtained by the domain-based method[48] is shown in Fig. 9, with all components having a cutoff radius of 2.0 Å. With the increase of K_2O content, the occupancy proportions of cavities of $x{}^{11}K_2O{\cdot}(1-x){}^{11}B_2O_3$ (x = 0.10, 0.20, 0.30, and 0.40) glass are 7.3%, 6.9%, 5.6%, and 5.2%, respectively, where the cavity volumes are 399, 379, 277 and 234 Å^3, respectively. The cavities show a decreasing trend in cavity occupancy. This phenomenon of decreasing cavity occupancy with an increase of metal ion content also exists in sodium thioarsenate and silver thioarsenate glass.[58–60]

3.3 Transport of K^+ in glassy materials

The study of the ion-transport pathway of K^+ in borate glassy materials and the structural factors that influence the ion-

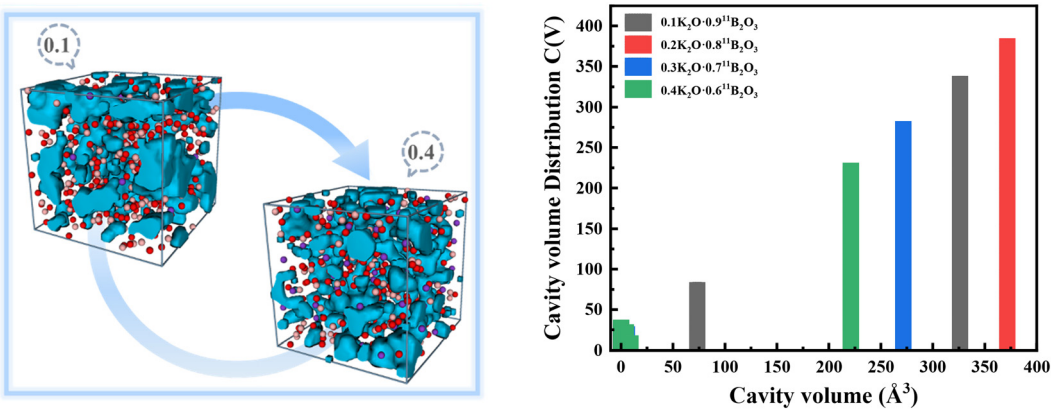

Fig. 9 The distribution of cavities (left) and the cavity volume distribution histogram (right) for $x{}^{11}K_2O{\cdot}(1-x){}^{11}B_2O_3$ ($0.1 \leq x \leq 0.4$) glass.

transport rate are essential for improving the performance of potassium solid-state batteries and developing new K^+ batteries. Fig. S8† shows an animation of the K^+ transport process in the $0.40K_2O{\cdot}0.60^{11}B_2O_3$ glassy material. An interesting phenomenon observed is that the transport pathways and sites for adjacent K^+ ions are almost identical. However, the transmission rate of K^+ during the transmission process is affected by the boron–oxygen network structure. The structural reasons that affect the transport path and rate of potassium ions are analyzed in the following content.

Fig. 10(a) shows the time trajectory of four K^+ ions at the 150th frame. The denser the trajectory points, the slower the ion transport. According to Fig. S8,† the transport of 1# and 3# K^+ is slow, and the transport of 2# and 4# K^+ is faster. This study suggests that the structural factors influencing the K^+ transport rate may include the following points. (1) coordination number and type of K^+: Fig. 10(b) shows the coordination distribution of four types of K^+ ions at frame 150. The NBO/CN ratios (the number of NBOs coordinated with K^+ divided by the total coordination number of that K^+) of 1 to 4# K^+ are 0, 1, 0.4, and 0.4, respectively. Therefore, one of the structural reasons for the faster transport rate of 2# compared to 1# K^+ is that all oxygen atoms coordinated with 2# K^+ are NBOs. It is worth noting that 3# and 4# K^+ ions have the same NBO/CN ratio, but the transport rate of the 4# ion is significantly higher than that of 3# K^+. Therefore, besides coordination number and coordination type, there are other factors that influence ion transport. (2) Structural units: Fig. 10(c) shows the distribution of surrounding structural units for K^+ ions at the 150th frame. It can be observed that 3# K^+ is mainly surrounded by ring-type structures, such as six-membered rings containing $B\varnothing_4^-$ tetrahedra and complex eight-membered rings. On the other hand, 4# K^+ is mainly surrounded by simple chain-type structures, such as orthoborate units and metaborate units. Therefore, the presence of chain-type structures enhances the facilitation of K^+ transport. (3) Distribution of cavities: as shown in Fig. 10(d), 1# and 3# K^+ ions are at some distance from the adjacent cavity, so they transport slowly at first. In contrast, 2# and 4# K^+ ions are directly attached to the cavity, so they are initially transported faster. Akola *et al.*[59,60] also suggest that the cavities adjacent to Ag^+ serve as diffusion sites. The data at the 600th frame in Fig. S9† precisely verify the above analysis results.

In conclusion, the structural factors that influence K^+ transport in potassium borate glass are not singular but rather the result of multiple factors working together. Firstly, the content of NBOs plays a significant role, with a higher NBO content leading to faster K^+ transport. Secondly, the presence of chain-type structural units, such as metaborate rings and orthoborate chains, which predominantly contain NBOs, facilitates K^+ transport. It should be noted that these chain-type structural units are considered as "molecular-type" structures, as shown in Fig. S6.† The structural statistical results reveal the absence of "molecular-type" structures for x = 0.1 and 0.2, with the presence of only a limited number of $B\varnothing_2O^-$ chain structures observed for x = 0.3, while a significant abundance of metaborate units and orthoborate chains exist for x = 0.4. The distribution of cavity regions also plays a crucial role in ion transport dynamics. The availability of cavity structures surrounding K^+ is essential for diffusion, and a more homogeneous dis-

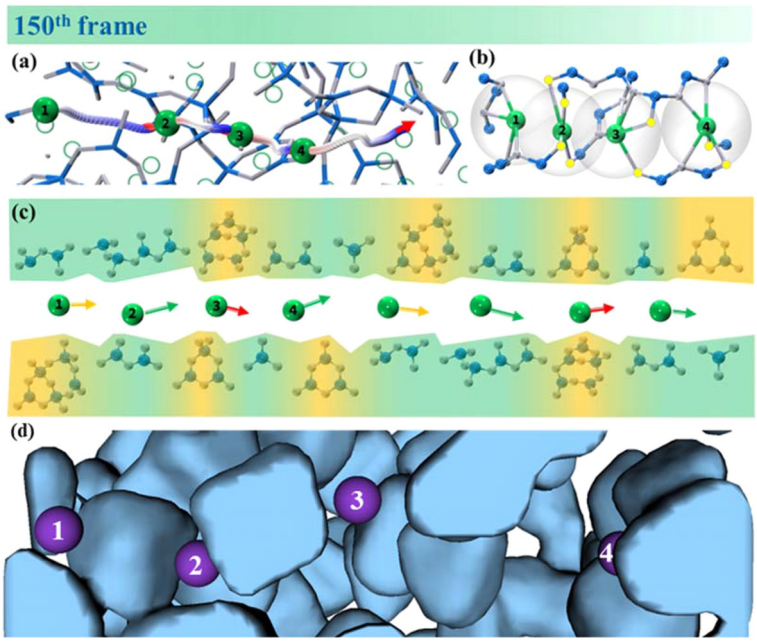

Fig. 10 Transport path of K^+ ions in $0.40K_2O{\cdot}0.60^{11}B_2O_3$ glass: (a) time trajectory diagram of K^+ at frame 150; (b) K–O coordination map at frame 150, with bright yellow spheres representing NBO; (c) the distribution of structural units around K^+ at frame 150; and (d) map of the cavity distribution around the four potassium atoms.

Table 2 Diffusion coefficient, error and fitting equations of K^+ in $xK_2O{\cdot}(1-x)^{11}B_2O_3$ ($0.1 \le x \le 0.4$) glass

Sample	D (cm^2 $s^{-1} \times 10^{-5}$)	Error (cm^2 $s^{-1} \times 10^{-5}$)	Equations
$0.10K_2O{\cdot}0.90^{11}B_2O_3$	3.13	0.040	MSD = 0.0013 × t − 0.48
$0.20K_2O{\cdot}0.80^{11}B_2O_3$	6.43	0.086	MSD = 0.0026 × t + 0.34
$0.30K_2O{\cdot}0.70^{11}B_2O_3$	13.25	0.075	MSD = 0.0053 × t − 1.48
$0.40K_2O{\cdot}0.60^{11}B_2O_3$	17.90	0.055	MSD = 0.0072 × t − 2.00

tribution of these regions facilitates efficient K^+ transport. Based on the findings of our analysis, this study employed AIMD simulations to calculate the diffusion coefficients of K^+ in $xK_2O{\cdot}(1-x)^{11}B_2O_3$ (x = 0.10, 0.20, 0.30, and 0.40) glasses as presented in Table 2, while the relevant fitting curves are as shown in Fig. S10.† It is evident from the results that the diffusion coefficients of K^+ ions gradually increase with an elevated content of K_2O in the glass. This conclusion further substantiates our previous analysis. In other words, the increase of the K_2O content in potassium borate glass leads to the increase in the NBO content (Fig. S4†) and the increase of chain structure, and the distribution of cavities became more and more uniform (Fig. 9). These structural changes all contributed to the transport of potassium ions and increased the diffusion coefficient of potassium ions under the action of an electric field. The positive correlation between the contents of NBO and the chain-structure units in potassium borate glass on the transport rate of K^+ ions was established. The study of Kamitsos *et al.*[61] showed that the diffusion of Li^+ in lithium borate glass is mainly through the NBO site and, in the range of $0.2 \le x$ (mol Li_2O%) ≤ 0.4, with the increase of lithium oxide content, the content of NBO also increases, and the diffusion coefficient of the lithium ion also shows an increasing trend, which is the same as that of potassium-ion diffusion in potassium borate glass.

4. Conclusions

In potassium borate glass, with the increase of K_2O content, $B\varnothing_3$ content decreases, $B\varnothing_4^-$ content increases first and then decreases, and $B\varnothing_{(3-a)}O_a^{a-}$ (a = 1 or 2) content increases. With the increase of $B\varnothing_4^-$, the three-dimensional connectivity of the network structure of the glass is enhanced. With the increase of $B\varnothing_{(3-a)}O_a^{a-}$ (a = 1 or 2), the content of NBO also increases, and the structure of the boron–oxygen network becomes dispersed. The maximum point of $B\varnothing_4^-$ content (x = 0.3) is also the point with the highest number of rings, density and atomic density. Potassium borate glass contains more B–O bond types than crystals with similar components, and the bond lengths of ^{3}B–BO, ^{4}B–BO and ^{3}B–NBO are longer than those of corresponding crystals, so the boron–oxygen network structure is looser than that of crystals with similar components. Additionally, both the crystal and glass exhibited a reduction in the B–O bond length with an increase in NBO, while an increase in ^{4}B resulted in the elongation of the B–O bond.

The structural factors affecting the K^+ transport rate in $xK_2O{\cdot}(1-x)^{11}B_2O_3$ (x = 0.10, 0.20, 0.30, 0.40) glass mainly include: (1) NBO content, where the higher the value, the faster the K^+ transport. (2) Chain structure unit, where the greater the number of chain-type structural units, the faster the K^+ transport. (3) Cavity distribution, where the more uniform the cavity distribution, the more conducive it is to K^+ transport. With the increase of K_2O content, the diffusion coefficient of K^+ in glass increases gradually. This study provides reference information for understanding the structure of potassium borate glass and for designing and preparing a solid potassium-ion glass electrolyte.

Author contributions

Lulu Song performed sample preparation, characterization, *ab initio* molecular dynamics simulation, data analysis and manuscript writing. Alex C. Hannon performed neutron diffraction experiments and manuscript revision. Steve Feller participated in manuscript revision and sample preparation. Ruirui Liu participated in *ab initio* molecular dynamics simulation. Peyton McGuire participated in sample preparation. Bo Zhang participated in data analysis. Yongquan Zhou participated in manuscript revision. Wu Li supervised and revised the manuscript., Fayan Zhu designed and supervised the study, and revised manuscript.

Conflicts of interest

There are no conflicts to declare.

Acknowledgements

The authors thank the Qinghai Province innovation platform construction project (no. 2024-ZJ-T01), the US National Science Foundation (DMR-RUI 2203142), and the Qinghai Province "High-end Innovative Talents Plan" (E240HX1001) project for financial support, and also thank the Science and Technology Facilities Research Council (STFC) for beam time on SANDALS (No. 2010510).

References

1 E. O. Taha and A. Saeed, *Sci. Rep.*, 2023, **13**, 12260.
2 A. E. Harby, A. E. Hannora, A. M. Ali, *et al.*, *Sci. Rep.*, 2023, **13**, 12498.
3 A. R. Ghazy, B. M. Elmowafy, A. M. Abdelghany, *et al.*, *Sci. Rep.*, 2023, **13**, 7292.
4 M. Fayaz, S. Ali, S. Bibi, *et al.*, *Ceram. Int.*, 2023, **49**, 24690–24695.

5 J. Banerjee, G. Ongie, J. Harder, *et al.*, *J. Non-Cryst. Solids*, 2006, **352**, 674–678.
6 J. F. Wang and P. Liang, *J. Chem. Thermodyn.*, 2019, **134**, 1–4.
7 A. M. A. Ghany, A. S. A. Khadra and M. S. Sadeq, *J. Non-Cryst. Solids*, 2020, **548**, 120320.
8 M. I. Sayyed, M. A. Abdo, H. E. Ali, *et al.*, *Ceram. Int.*, 2022, **48**, 24310–24318.
9 S. A. M. Issa, M. Ahmad, H. O. Tekin, *et al.*, *Results Phys.*, 2019, **13**, 102165.
10 M. I. Sayyed, M. A. Abdo, H. E. Ali, *et al.*, *Ceram. Int.*, 2022, **48**, 30817–30825.
11 H. Aboud, H. Wagiran, R. Hussin, *et al.*, *Appl. Radiat. Isot.*, 2014, **90**, 35–39.
12 B. Pandit, E. S. Goda, M. Ubaidullah, *et al.*, *Ceram. Int.*, 2022, **48**, 28856–28863.
13 R. Balaji Rao, R. A. Gerhardt and N. Veeraiah, *J. Phys. Chem. Solids*, 2008, **69**, 2813–2826.
14 A. E. Omar, A. M. Ibrahim, T. H. Abd El-Aziz, *et al.*, *J. Biomed. Mater. Res., Part B*, 2021, **109**, 1059–1073.
15 R. E. Youngman and J. W. Zwanziger, *J. Phys. Chem.*, 1996, **100**, 16720–16728.
16 W. L. Konijnendijk and J. M. Stevels, *J. Non-Cryst. Solids*, 1975, **18**, 307–331.
17 E. Kamitsos, M. A. Karakassides and G. D. Chryssikos, *Phys. Chem. Glasses*, 1989, **30**, 229–234.
18 G. D. Chryssikos, E. Kamitsos and M. A. Karakassides, *Phys. Chem. Glasses*, 1990, **31**, 109–116.
19 A. A. Osipov, L. M. Osipova and R. T. Zainullina, *Phys. Chem. Glasses: Eur. J. Glass Sci. Technol., Part B*, 2015, **56**, 248–254.
20 O. N. Koroleva and M. V. Shtenberg, *J. Non-Cryst. Solids*, 2023, **601**, 122053.
21 A. C. Wright, R. N. Sinclair, C. E. Stone, *et al.*, *Phys. Chem. Glasses: Eur. J. Glass Sci. Technol., Part B*, 2012, **53**, 191–204.
22 K. Handa, Y. Kitab, S. Kohara, *et al.*, *J. Phys. Chem. Solids*, 1999, **60**, 1465–1471.
23 B. Stevensson, Y. Yu and M. Edén, *Phys. Chem. Chem. Phys.*, 2018, **20**, 8192–8209.
24 G. D. Chryssikos, E. I. Kamitsos, A. P. Patsis, *et al.*, *J. Mater. Sci. Eng. B*, 1990, **7**, 1–4.
25 E. I. Kamitsos and G. D. Chryssikos, *J. Mol. Struct.*, 1991, **247**, 1–16.
26 T. Liu, B. Duan, Y. Q. Li, *et al.*, *J. Non-Cryst. Solids*, 2023, **604**, 122134.
27 V. Dua, S. K. Arya and K. Singh, *J. Mater. Sci.*, 2023, **58**, 8678–8699.
28 S. C. Colak and G. Kilic, *J. Mater. Sci.: Mater. Electron.*, 2022, **33**, 21852–21863.
29 N. Effendy, H. A. A. Sidek and M. K. Halimah, *Chin. J. Phys.*, 2022, **75**, 1–13.
30 L. L. Song, Y. X. Wang, A. C. Hannon, *et al.*, *J. Non-Cryst. Solids*, 2023, **616**, 122478.
31 H. Bradtmüller, A. Gaddam, H. Eckert, *et al.*, *Acta Mater.*, 2022, **240**, 118318.
32 E. D. Zanotto, J. E. Tsuchida, J. F. Schneider, *et al.*, *Int. Mater. Rev.*, 2015, **60**, 376–391.
33 S. Lan, L. Zhu, Z. Wu, *et al.*, *Nat. Mater.*, 2021, **20**, 1347–1352.
34 J. Ge, Y. Gu, Z. Yao, *et al.*, *J. Mater. Sci. Technol.*, 2024, **176**, 224–235.
35 A. C. Hannon, *Nucl. Instrum. Methods Phys. Res., Sect. A*, 2005, **551**, 88–107.
36 A. Hannon, W. Howells and A. Soper, *Inst. Phys. Conf. Ser.*, 1990, 193–211.
37 E. Lorch, *Phys. Solid State*, 1969, **2**, 229.
38 A. C. Hannon, *J. Non-Cryst. Solids*, 2016, **451**, 56–67.
39 A. C. Hannon, A. S. Gibbs and H. Takagi, *J. Appl. Crystallogr.*, 2018, **51**, 854–866.
40 J. Hutter, M. Iannuzzi, F. Schiffmann, *et al.*, *WIREs Comput. Mol. Sci.*, 2014, **4**, 15–25.
41 Z. Wu and R. E. Cohen, *Phys. Rev. B: Condens. Matter Mater. Phys.*, 2006, **73**, 235116.
42 L. Martínez, R. Andrade, E. G. Birgin, *et al.*, *J. Comput. Chem.*, 2009, **30**, 2157–2164.
43 D. V. Oliveira, J. Laun, M. F. Peintinger, *et al.*, *J. Comput. Chem.*, 2019, **40**, 2364–2376.
44 S. Goedecker, M. Teter and J. Hutter, *Phys. Rev. B: Condens. Matter Mater. Phys.*, 1996, **54**, 1703.
45 S. Nosé, *Mol. Phys.*, 1984, **52**, 255–268.
46 W. G. Hoover, *Phys. Rev. A: At., Mol., Opt. Phys.*, 1985, **31**, 1695.
47 S. Le Roux and P. Jund, *Comput. Mater. Sci.*, 2010, **49**, 70–83.
48 I. Heimbach, F. Rhiem, F. Beule, *et al.*, *J. Comput. Chem.*, 2017, **38**, 389–394.
49 W. Humphrey, A. Dalke and K. Schulten, *J. Mol. Graphics Modell.*, 1996, **14**, 33–38.
50 A. K. Soper, *Phys. Rev. B: Condens. Matter Mater. Phys.*, 2005, **72**, 104204.
51 A. Hannon, D. Grimley, R. Hulme, *et al.*, *J. Non-Cryst. Solids*, 1994, **177**, 299–316.
52 P. A. Johnson and A. C. Wright, *J. Non-Cryst. Solids*, 1982, **50**, 281–311.
53 R. L. Mozzi and B. E. Warren, *J. Appl. Crystallogr.*, 1970, **3**, 251–257.
54 N. P. Lower, J. L. McRae, H. A. Feller, *et al.*, *J. Non-Cryst. Solids*, 2001, **293**, 669–675.
55 G. Lelong, L. Cormier, L. Hennet, *et al.*, *Inorg. Chem.*, 2021, **60**, 798–806.
56 E. I. Kamitsos, A. P. Patsis and G. D. Chryssikos, *J. Non-Cryst. Solids*, 1993, **152**, 246–257.
57 J. H. Zhong and P. J. Bray, *J. Non-Cryst. Solids*, 1989, **111**, 67–76.
58 M. Kassem, T. Bounazef, D. Fontanari, *et al.*, *Inorg. Chem.*, 2020, **59**, 16410–16420.
59 J. Akola, P. Jóvári, I. Kaban, *et al.*, *Phys. Rev. B: Condens. Matter Mater. Phys.*, 2014, **89**, 064202.
60 J. Akola, B. Beuneu, R. O. Jones, *et al.*, *J. Phys.: Condens. Matter*, 2015, **27**, 485304.
61 C. P. Varsamis, A. Vegiri and E. I. Kamitsos, *Phys. Rev. B: Condens. Matter Mater. Phys.*, 2002, **65**, 1–14.